Pergamon

PII: S0191-8141(97)00108-9

Journal of Structural Geology, Vol. 20, No. 4, pp. 417 to 431, 1998

0191-8141/98 $19.00 + 0.00

c-Axis fabrics and microstructures in a recrystallized quartz vein deformed under fluid-rich greenschist conditions

TORU TAKESHITA and IKUO HARA

Department of Earth and Planetary Systems Science, Faculty of Science, Hiroshima University, Higashi-Hiroshima, 739, Japan

(*Received* 18 *November* 1996; *accepted in revised form* 3 *November* 1997)

Abstract—The quartz *c*-axis orientations and microstructures have been analyzed in an originally single-crystal buckled quartz vein of greenschist metamorphic grade from the Sambagawa metamorphic belt, southwest Japan. The basal (0001) plane was inclined by *ca* 10–20° to the quartz vein surface before deformation, and the flexure (essentially kink) which produced the fold was accomplished by basal (0001) slip alone in the hinges (i.e. flexural-slip folding). In addition to crystal plasticity, dissolution microstructures are ubiquitous in the quartz vein. Dynamic recrystallization resulted from both subgrain rotation and grain-boundary migration. Rotation recrystallization associated with basal (0001) slip resulted in host-controlled *c*-axis orientation distribution along a great circle, whereas migration recrystallization, perhaps assisted by intergranular fluid, resulted in a penetrative development of a weak *X* (elongation)-maximum *c*-axis fabric nowhere rotated by the folding. The migration recrystallization is evidenced by large *c*-axis misorientations across the grain boundaries, as well as irregular grain shape. Based on the weak *c*-axis fabric development and lack of grain shape fabric, solution-precipitation creep may have dominated in the fluid-assisted grain-boundary migration regime, and hence it is inferred that the transition from rotation to migration recrystallization was caused by a local decrease of differential stress in the buckled quartz vein. © 1998 Elsevier Science Ltd. All rights reserved

INTRODUCTION

The role of dynamic (syn-tectonic) recrystallization in developing lattice-preferred orientation (LPO) in quartz has long been an enigma (e.g. Hobbs, 1968). In order to understand the LPO development, it is necessary to know the mechanism of dynamic recrystallization. It is well known that there are two different mechanisms of dynamic recrystallization: subgrain rotation (or rotation recrystallization); and grain-boundary migration (migration recrystallization) (e.g. Guillope and Poirier, 1979). The kinematically induced LPO in quartz polycrystals resulting from intracrystalline slip, which can be simulated by the Taylor–Bishop–Hill model (e.g. Lister *et al.* 1978; Takeshita and Wenk, 1988), is not greatly modified by rotation recrystallization because the lattice orientations of recrystallized grains are controlled by those of the host grains. For rotation recrystallization it is even possible to identify the operative slip systems based on the crystallographic orientation distribution in recrystallized grains, as recently demonstrated by Lloyd and Freeman (1991, 1994) using the SEM electron channeling technique. On the other hand, the LPO resulting from migration recrystallization (or grain growth) may be completely different from one caused by intracrystalline slip, and possibly controlled by stress state (e.g. Kamb, 1959, 1961; Karato, 1987).

For experimentally deformed quartz aggregates, Hirth and Tullis (1992) and Gleason *et al.* (1993) have recently identified three regimes of dislocation creep and dynamic recrystallization under physical conditions roughly comparable with natural greenschist-facies conditions. *c*-Axis fabrics, such as small circle girdles, and recrystallization microstructures in natural quartz aggregates deformed under greenschist-facies conditions (e.g. Bouchez, 1977; Law, 1986) are well correlated with those for either regime 2 or 3 of Hirth and Tullis (1992), where dynamic recrystallization primarily occurred by subgrain rotation. However, in natural quartz aggregates deformed under fluid-rich greenschist-facies conditions, where dissolution of minerals are pervasive, another type of quartz *c*-axis fabric, an *X*-maximum pattern (namely, *c*-axes parallel to stretching direction) has recently been found (Hippertt, 1994; Stallard and Shelley, 1995), although under amphibolite-granulite facies conditions an *X*-maximum *c*-axis fabric was produced by dominant *c*-slip (e.g. Blumenfeld *et al.*, 1986; Okudaira *et al.*, 1995). The development of *X*-maximum *c*-axis fabrics under fluid-rich greenschist conditions may suggest a different regime of deformation and recrystallization in quartz.

In this study, a thorough investigation of *c*-axis fabrics and microstructures in a dynamically recrystallized quartz vein deformed under fluid-rich greenschist-facies conditions has been conducted. Through the microstructural analyses, we demonstrate that both rotation and migration recrystallization operated in the same quartz vein, resulting in the development of host-controlled and *X*-maximum *c*-axis fabrics, respectively. Further, a possible cause for the transition between the two recrystallization mechanisms is suggested.

GEOLOGICAL SETTING AND SAMPLE DESCRIPTION

A folded pelitic schist sample was selected for the present study from the chlorite zone of the Sambagawa metamorphic belt in central Shikoku, Japan, a well-known high P–T metamorphic belt metamorphosed and exhumed in Cretaceous time (e.g. Isozaki and Itaya, 1990; Takasu and Dallmeyer, 1990). For a general outline of the Sambagawa metamorphic belt in central Shikoku see, for example, Banno and Sakai (1989) and Hara *et al.* (1990).

In the Sambagawa metamorphic belt in central Shikoku, open folds with W- to WNW-trending and horizontally plunging axes and vertically dipping axial planes were developed particularly in the chlorite zone. The fold system formed during the Hijikawa (D_3) phase (latest Cretaceous–earliest Tertiary) (e.g. Hara *et al.*, 1977; Faure, 1985), and a quartz vein buckled during the D_3 phase was analyzed in the present study. It has been estimated that by the D_3 phase, the Sambagawa metamorphic rocks were already exhumed above *ca* 5 km (i.e. less than 2 kbar) (e.g. Banno and Sakai, 1989; Hara *et al.*, 1992). The temperature conditions during the D_3 phase have recently been estimated as *ca* 300–350°C based on the homogenization temperatures of fluid inclusions in quartz (Seki *et al.*, 1993; unpublished data of Naomoto, 1994).

The orientations of the principal strain axes in the D_3 phase folds have been inferred by Hara *et al.* (1968), Hara (1971) and Hara and Paulitsch (1971), based on both the three-dimensional shape and the *c*-axis fabric patterns of recrystallized quartz grains. According to their studies, the elongation (X), intermediate (Y) and shortening (Z) directions are parallel to the axial plane and normal to the fold axis (i.e. vertical), parallel to the fold axis, and normal to the axial plane, respectively.

In a thin section cut normal to the fold axis (Y-direction) (i.e. XZ section), a few quartz veins (their thickness is less than 2 mm) parallel to the foliation (defined by preferred alignment of muscovite) are folded together with muscovite layers (Fig. 1). The fold is asymmetrical with the ratio of limb length more than 1:4. Associated with the fold are crenulation folds and crenulation (solution) cleavages, which are also apparent in the outcrop.

VARIATIONS IN THE c-AXIS ORIENTATION THROUGHOUT THE BUCKLED QUARTZ VEIN

Variations in the c*-axis orientation in the host grains*

The *c*-axis orientations of almost all the host and recrystallized grains in the buckled quartz vein were measured with a U-stage. The analyzed buckled quartz vein was divided into two parts, I and II (Fig. 1). In this paper, all the portions in the buckled quartz vein, namely parts, limbs and recrystallized domains are numbered in numerical (Roman), alphabetical (lowercase letter) and alphabetical (capital letter) orders, respectively, from right to left throughout. Whereas in part I, recrystallization is only extensive in the sharply bent hinge (Fig. 2) and host grains are preserved in most places, part II is completely recrystallized. Three limbs constituting a wave of the fold in part I are referred to as limbs a, b and c, respectively (Fig. 2). Limb b is slightly bent near the boundary between the recrystallized and host domains, and therefore further divided into limbs b1 and b2 (Fig. 2). Stereographic plots of the host *c*-axis orientations in the three limbs (a, b1 and c) are shown in Fig. 3 (host grains) together with the orientations of the three limbs, XY plane of finite strain and poles to crenulation cleavages. The orientation of the XY plane of finite strain was determined by the average orientation of crenulation cleavages, and nearly parallel to the axial plane.

The interlimb angles between limbs a and b1, and limbs b1 and c are 102° and 93°, respectively. This means that limb b1 is rotated clockwise by 78° about the fold axis with respect to limb a, while limb c is rotated counterclockwise by 87° with respect to limb b1. The host *c*-axis orientations in limb b1 are rotated clockwise by *ca* 75° from those in limb a, while those in limb c are rotated counterclockwise by *ca* 80° from those in limb b1 about the fold axis. The coincidence of the rotation angles between the vein and host *c*-axis orientations indicates that the host grains in limbs a, b1 and c all originated as a single crystal with its basal plane inclined by *ca* 10–20° with respect to the vein surface (Fig. 4), and that the orientation difference of the *c*-axes was caused solely by buckling.

c-*Axis orientation distribution in the recrystallized grains of part I*

While the *c*-axis orientations in recrystallized grains for each domain B–E (Fig. 2) are plotted on equal-area projections, they are also shown directly on each grain (Fig. 3, here referred to as the map of *c*-axis orientations). Here, three parallel linear recrystallized zones in limb b1 which are inclined by 40° to the limb are treated as a composite domain B (Fig. 2). In Fig. 3, only the azimuths of the *c*-axis orientations are shown, because most of the *c*-axis orientations make small angles (less than 30°) with the projection plane (XZ section). Furthermore, a schematic trace of basal (0001) plane is drawn in Fig. 4 based on the map of *c*-axis orientations.

Domain A, which is located at the hinge zone between limbs a and b1 (Fig. 2), was heavily kinked although not recrystallized. Note that the *c*-axis orientations in domain A are nearly parallel to the kink band boundaries. The *c*-axis orientations across

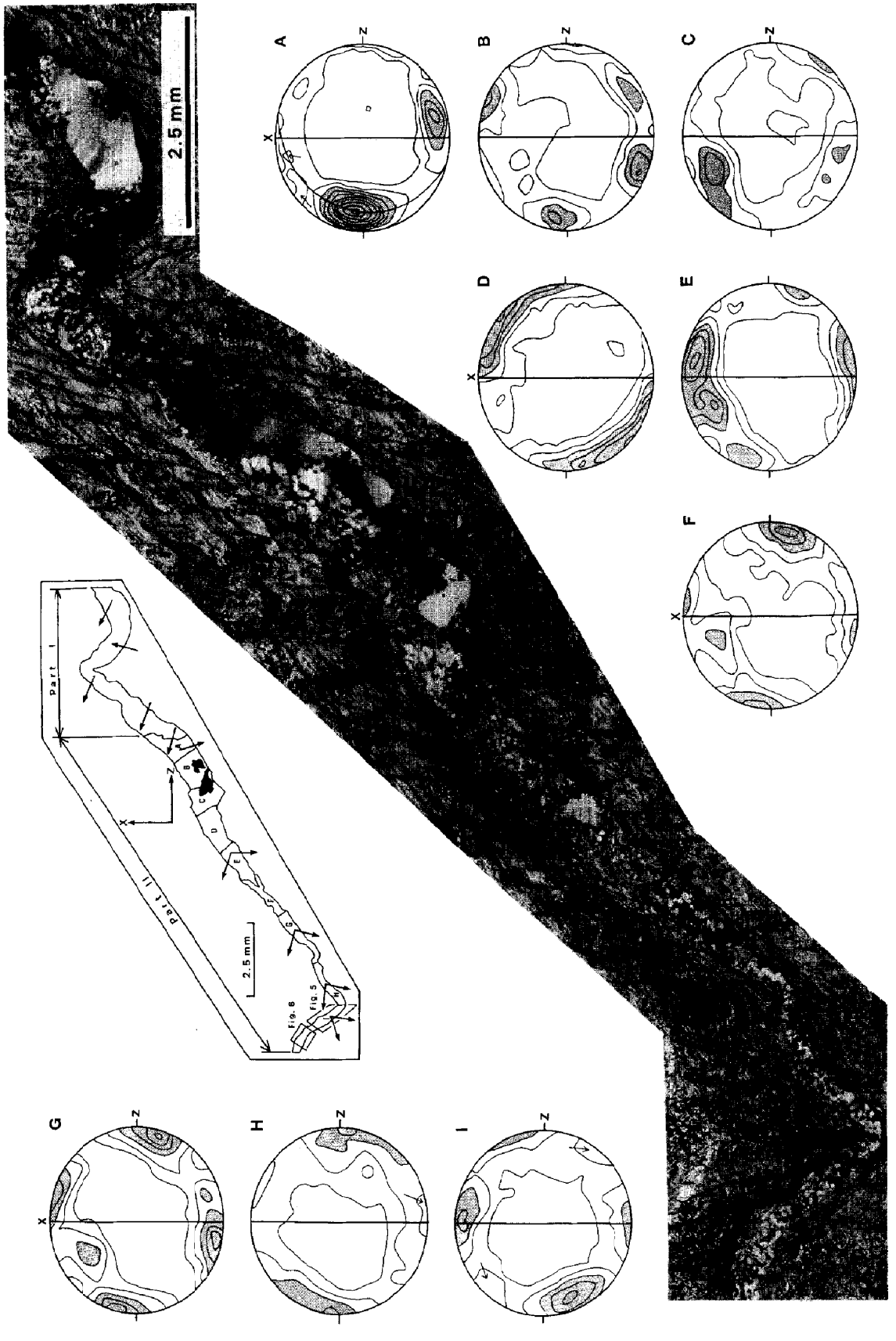

Fig. 1. Micrograph of the pelitic schist sample analyzed in the study. Note that the analyzed quartz vein is folded together with muscovite layers. There is a penetrative development of crenulation (solution) cleavage in the mica-rich matrix. An inset diagram shows a sketch of the buckled quartz vein. Parts I and II are indicated; A–I indicate the recrystallized domains of part II. Arrows indicate general trends of the *c*-axis orientations. Black denotes holes in the thin section. Also shown are *c*-axis fabric diagrams for recrystallized domains in part II of the buckled quartz vein. The number of *c*-axis orientations is 250 for each diagram. Kamb contours and contour intervals are 2σ, and are shaded above 6σ. Equal-area and lower-hemisphere projections in *XZ* section. N–S straight lines denote the *XY* plane of finite strain in the buckled quartz vein. The *c*-axis orientation in the nearest host grain is shown only in diagram A by an open circle. Curved solid line and open square in A indicate the best fit great circle for the *c*-axis orientation distribution and pole to the great circle, respectively. See text for further explanations.

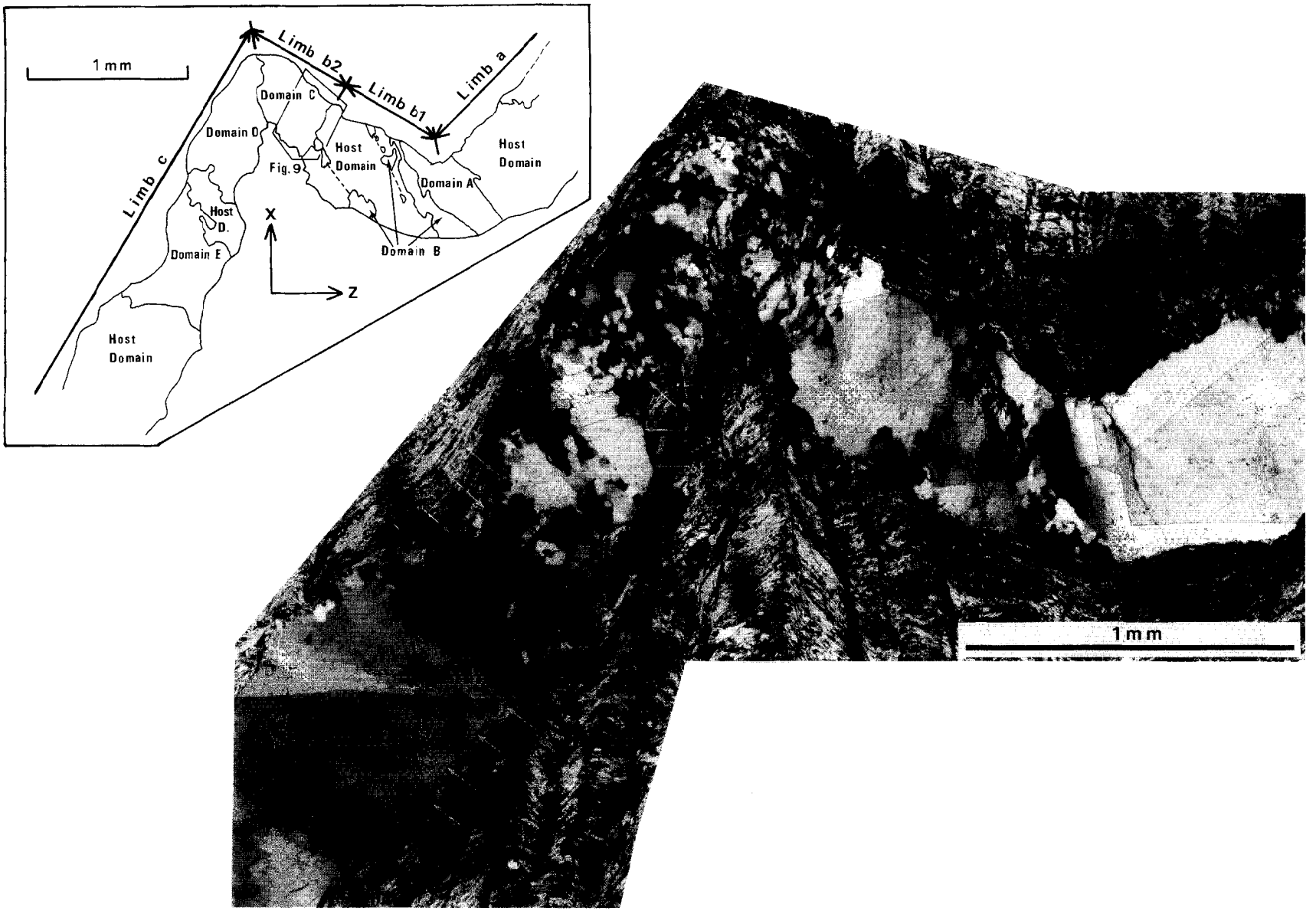

Fig. 2. Micrograph of part I of the buckled quartz vein. Note the penetrative development of crenulation (solution) cleavages in the mica-rich matrix. Some of undulations of the quartz vein surface indicating dissolution of the quartz are shown by arrows. An inset diagram shows a sketch of part I of the buckled quartz vein. Division of the limbs, host domains, kinked domain A and recrystallized domains B E are indicated.

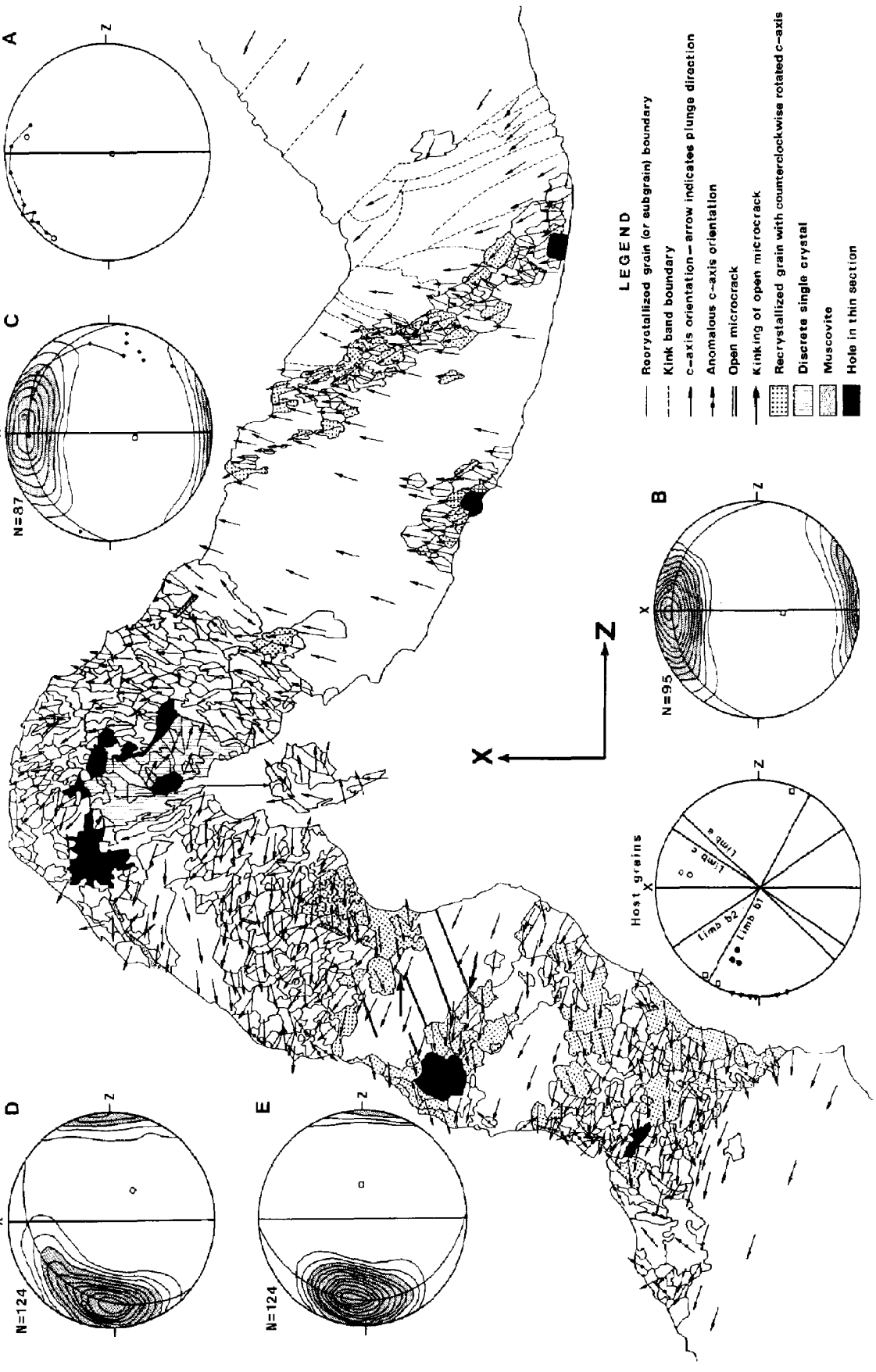

Fig. 3. c-Axis orientations of the individual host and recrystallized grains in part I of the buckled quartz vein (map of the c-axis orientations). Dotted grains have c-axis orientations which are rotated counterclockwise by more than 15° about the fold axis with respect to those in adjacent host or recrystallized grains. Stereographic lower-hemisphere projections of the host c-axis orientations (host grains) in limbs a (open square), b1 (open circle) and c (solid circle) are presented together with the orientations of each limb, the *XY* plane of finite strain and poles to the crenulation cleavages (solid triangles). Lower-hemisphere projections of the c-axis orientation distributions in domains I.A–I.E are shown. A: stereographic projection, B–E: equal-area projections. For contours, see captions of Fig. 1. In C, the c-axis orientations in the discrete single crystal are shown by dots. For the kinked domains, I.A and that in the discrete single crystal (C), the c-axis orientations in adjacent grains are connected by partial great circles. N–S straight lines and open circles denote the *XY* plane of finite strain in the buckled quartz vein, and the c-axis orientations in the nearest host grains, respectively. Curved solid lines and open squares indicate the best-fit great circle for the c-axis orientation distribution and pole to the great circle, respectively. See text for further explanations.

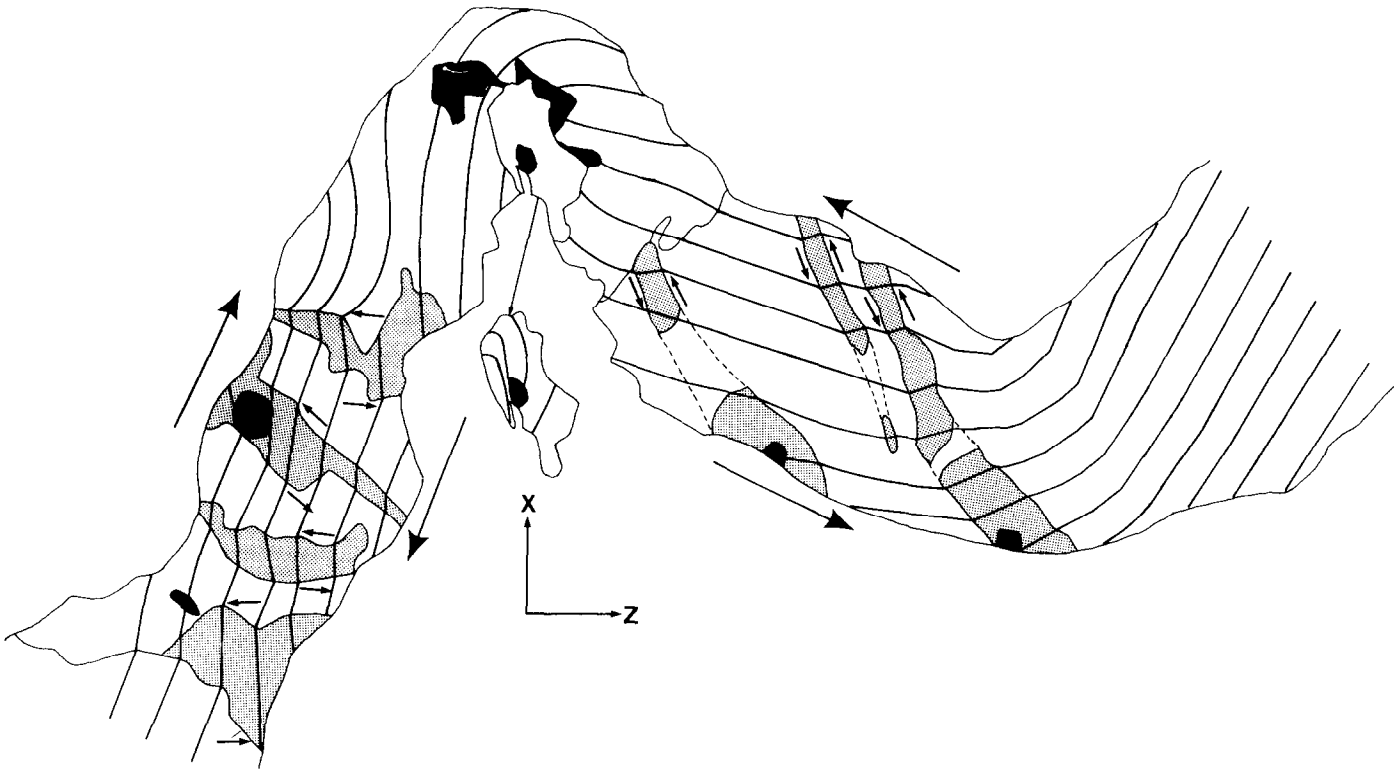

Fig. 4. The basal (0001) plane traces in the buckled quartz vein. Shaded areas indicate recrystallized zones, perhaps evolved from kink bands, with c-axes rotated counterclockwise about the fold axis with respect to the host c-axis orientation. Large and small arrows denote the sense of slip for the flexural-slip folding of the quartz vein, and that for the formation of the inferred kink bands, respectively. Black denotes holes in the thin section. See text for detailed explanation.

domain A are progressively rotated by kinking along a great circle about the fold axis from the host c-axis orientation in limb a to that in limb b1 (Fig. 3).

The c-axis orientation distributions of recrystallized grains in all the other domains (B, C, D and E) are similar and characterized by a cluster around the host c-axis orientations (Fig. 3). All of the c-axis orientations are rotated along a great circle about an axis nearly parallel to the fold axis. Note in domain C that the c-axis orientations are gradually rotated counterclockwise about the fold axis from the limb to the outer hinge (Fig. 3). In domains B, D and E, it is clear from both the equal-area projections and map of c-axis orientations that the recrystallized grains with c-axis orientations rotated counterclockwise dominate over those with c-axis orientations rotated clockwise about the fold axis with respect to the host c-axis orientations, and the recrystallized grains with the counterclockwise rotated c-axes seem to constitute linear zones (Figs 3 & 4).

In domain C, there is a small region located at the inner hinge of the fold within which the c-axis orientations of host and recrystallized grains are completely different from the majority of the c-axis orientations (Fig. 3). The discrete c-axis orientations in this small region seem to represent those of another original single crystal, and they are greatly rotated by kinking along a great circle about the fold axis (Fig. 3).

In domains D and E, there are anomalously oriented grains (shown by arrows with dots in Fig. 3), the c-axis orientations of which differ greatly from the host-controlled c-axis orientations in the majority of grains. In the anomalously oriented grains, which are mostly located at the outer folded surface, the c-axes are dominantly oriented both parallel to the local orientations of crenulation cleavages (Fig. 2) and perpendicular to the fold axis (hence parallel to X-direction).

c-*Axis orientation distribution in the recrystallized grains of part II*

In part II of the quartz vein, the c-axis orientations in recrystallized grains were plotted on equal-area projections for every 250 grains, which constitute the recrystallized domains A–I (Fig. 1). First of all, the intensity of c-axis fabrics in part II is much weaker than in part I; the maximum concentration of c-axis fabrics in different domains of part II is less than 5 m.u.d. (multiples of a uniform distribution) compared to more than 10 m.u.d. in part I.

Recrystallized domains A of part II (here referred to as II.A) and E of part I (I.E) both evolved from the

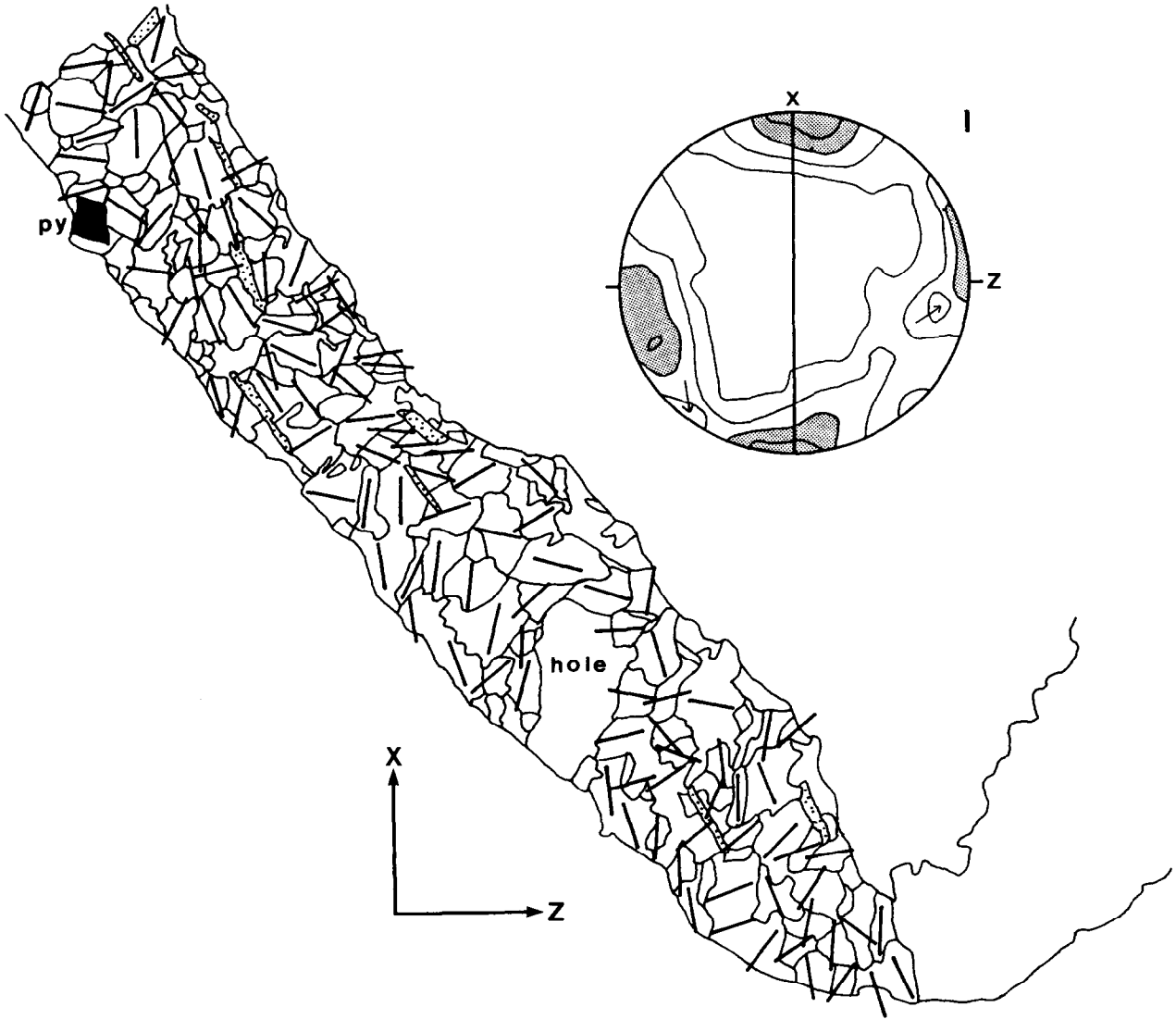

Fig. 5. Map of the c-axis orientations in a part of recrystallized domain II.I of the buckled quartz vein. Location is indicated in the inset diagram of Fig. 1. Only the azimuths of the c-axis orientations are shown (bars). Dots and black (py) indicate muscovite and pyrite, respectively. Also shown is the lower-hemisphere, equal-area projections of the c-axis orientations. For contours, see captions of Fig. 1.

same host grain. The host-controlled maximum of c-axis orientations oriented nearly perpendicular to the XY plane (Z-maximum) was developed in both domains, and both the c-axis orientations are rotated along a great circle about an axis nearly parallel to the fold axis (compare A in Fig. 1 with E in Fig. 3). On the other hand, another maximum nearly parallel to the elongation direction (X-maximum) was only developed in domain II.A. Both the Z- and X-maxima were penetratively developed throughout the domains from II.A to I. However, the X-maximum seems to be split in domain II.B, and another discrete maximum which is rotated counterclockwise by 25–32° from the X-axis about the fold axis and plunging by 30–35° towards the X-axis, was developed in addition to the X-maximum component in domains II.C, II.E, II.F and II.G (Fig. 1).

Because the recrystallized grains belonging to the different c-axis orientation groups are often adjacent each other (Figs 5 & 6), the c-axis misorientation between recrystallized grains in part II is often very large, larger than 60° and as much as 90°. Axial distribution analysis (AVA; Sander, 1934) was carried out for a part of domain II.I (Fig. 6b). The analysis has revealed that the grains with their c-axis dominantly oriented nearly parallel to the X-axis grew into the originally large host grains with their c-axis oriented nearly parallel to the Z-axis (shaded in Fig. 6b) which were polygonized and kinked during the folding.

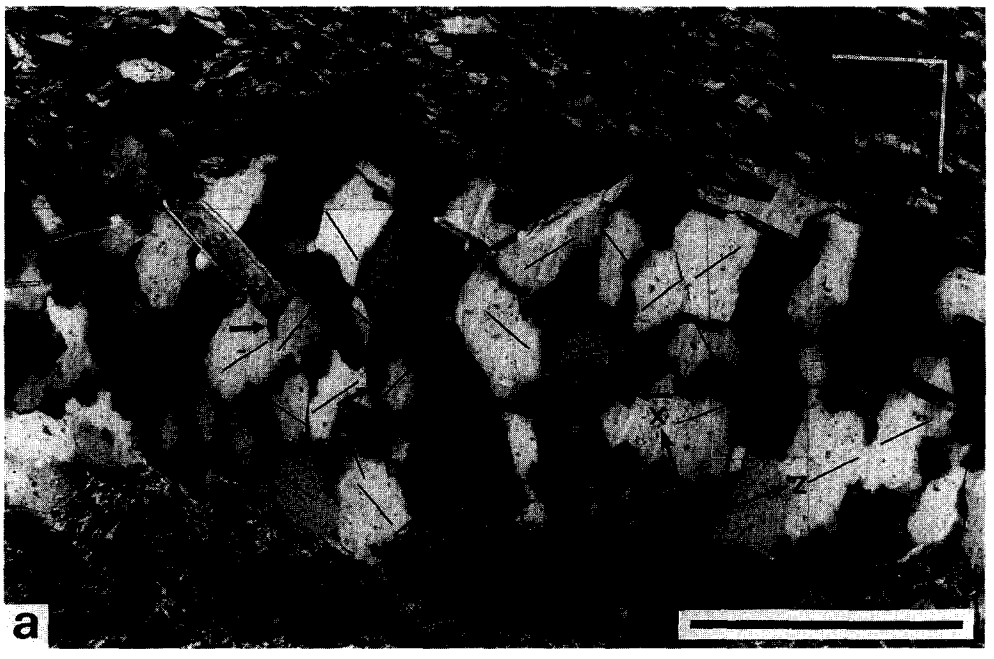

(b)

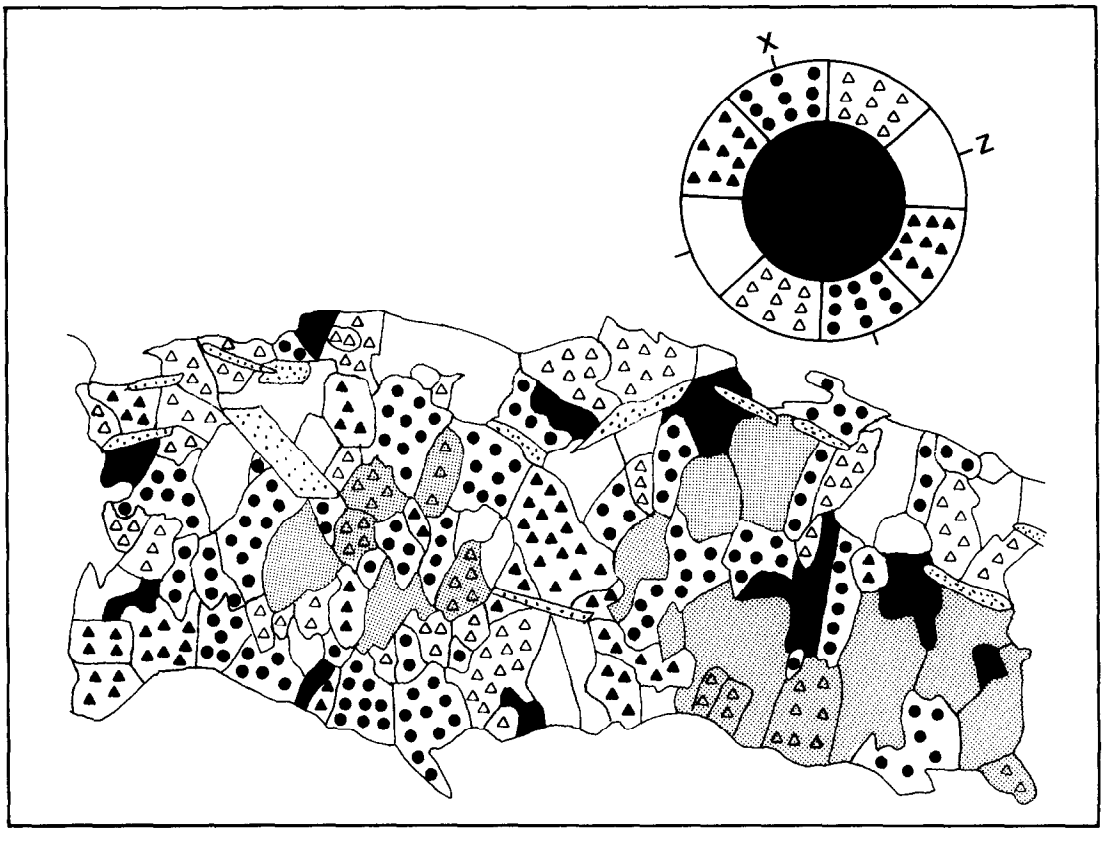

Fig. 6. Grain shape fabric in a part of recrystallized domain II.1 of the buckled quartz vein. Location is indicated in the inset diagram of Fig. 1. (a) Micrograph; bars indicate the azimuths of *c*-axis orientations in some of the recrystallized grains. Note irregularly shaped grains and lobate shape of the grain boundaries shown by arrows. Vibration directions of crossed nicols are indicated by thick bars. Scale bar 0.2 mm. (b) AVA diagram for the same area and magnification. It seems that the recrystallized grains exhibiting an *X*-maximum *c*-axis fabric grew, consuming those exhibiting a *Z*-maximum *c*-axis fabric. Dots indicate muscovite.

Domains II.H and II.I constitute the right and left limbs of a half wave of the fold, the interlimb angle of which is 80°. While the orientation of the Z-maximum was greatly rotated about the fold axis, perhaps due to the folding from domain II.H to II.I, the orientation of the X-maximum was little rotated by the folding from domain II.G through II.H to II.I (Fig. 1).

RECRYSTALLIZED GRAIN AND DISSOLUTION MICROSTRUCTURES

Size, shape and shape fabric of the recrystallized grains

The lengths of the longest and shortest axes (denoted as a and b, respectively) of the recrystallized grains were measured with a microscope for domains I.C and I.D, and domains II.H and II.I. The arithmetical mean recrystallized grain sizes (individual grain size calculated as $\sqrt{a \cdot b}$) are 22.3 and 32.1 μm in domains I.C and I.D, and domains II.H and II.I, respectively. The frequency distribution as a function of the logarithm of grain size approximately fits a normal distribution for both domains (Fig. 7). The arithmetical mean aspect ratio (individual grain aspect ratio calculated as a/b) is 2.3 in domains I.C and I.D, and 1.8 in domains II.H and II.I (Fig. 8).

For domains I.C and I.D, where grain shape fabric is conspicuous (Figs 2 & 9), an R_f/ϕ diagram (Dunnet, 1969) was constructed (Fig. 10a). Here, R_f and ϕ denote the aspect ratio, and angle between the longest axis of each recrystallized grain and the trace of the XY plane, respectively. Traces of the longest axis direction (Fig. 10b) show a convergent fan (Ramsay, 1967). The longest axis in the right limb near the outer hinge is sharply bent counterclockwise about the fold axis by as much as 90° which appears as 11 negative ϕ values in the R_f/ϕ diagram. On the other hand, the grain shape in part II is often very irregular, and lobate grain-boundaries with a large amplitude (Fig. 6a), possibly indicating a great extent of grain boundary migration, were developed at the boundaries of large c-axis misorientations. No shape fabric is discerned throughout part II (Figs 5 & 6).

Dissolution microstructures

Dissolution of quartz is extensive throughout the buckled quartz vein. The boundary between the quartz vein and mica-rich matrix (here referred to as the vein–matrix interface) is not straight, but rather undulating with many embayments, some of which are indicated by arrows in Fig. 2. The undulating vein–matrix interface is considered to be a dissolution front. In some localities, the dissolution process was significantly advanced to leave only lenticular grains as remnants of the quartz vein (Fig. 9).

DISCUSSION

Mechanism of folding in part I of the buckled quartz vein

The folding in part I was essentially accommodated by the formation of several kink bands in both the hinge part between limbs a and b1 (domain I.A), and the inner hinge part between limbs b2 and c. As the host c-axis orientations are rotated by kinking along a great circle in those hinge parts (A and C in Fig. 3), it is inferred that c-axis orientation was either the slip direction or normal direction of slip plane (e.g. Carter and Raleigh, 1969). Furthermore, as the host c-axes are parallel to the kink band boundaries (Fig. 3), it is inferred that the slip direction was perpendicular to the c-axis, possibly either in $\langle 2\bar{1}\bar{1}0\rangle$ ($\langle a\rangle$) or in $\langle 10\bar{1}0\rangle$ ($\langle m\rangle$) axis. Therefore, it is concluded that the operative slip plane was basal (0001) plane. As no other trends of the changes in host c-axis orientation are observed across the kink band boundaries, such as a 38° small circle for rhomb $\langle a\rangle$ and c-axis point maximum (i.e. no change) for prism $\langle a\rangle$ slip systems (e.g. Lloyd and Freeman, 1991, 1994), basal (0001) slip appears to have been the sole activated slip system.

Based on the fact that a mechanically weak basal (0001) plane initially nearly parallel to the single crystal quartz vein surface was just flexed (in reality bent by several kink bands at the hinge parts) to produce the fold (Fig. 4), it is concluded that the folding of the quartz vein was primarily accommodated by 'flexural slip', where the basal plane behaved as the flexural slip plane. The flexural-slip not only occurred in the hinges but also in the limbs (see below).

Why did grains in domains I.B and I.E (and part of domain I.D) in the limbs, which presumably have less strain than in the hinges, suffer strain-induced dynamic recrystallization? It has been noted that the recrystallized grains with c-axes showing counterclockwise rotations about the fold axis with respect to the host c-axis orientations, tend to occur in linear zones of a finite width surrounded by host grains or recrystallized grains with c-axis orientations similar to those of the host grains. Therefore, they were perhaps kinked (hence high strain) zones in the host grains, and the c-axis orientations in the linear recrystallized zones were inherited from those of the kinked host grains. If this is true, the shear sense along the kink bands can be inferred (Fig. 4). The inferred shear sense along the kink bands in domain I.B is synthetic to the sense of flexural slip associated with the folding of the quartz vein (shown by large arrows in Fig. 4), while that in domains I.D and I.E is all antithetic (conjugate), also confirmed by the shear sense of slightly kinked open microcracks (shown by large arrows in Fig. 3) developed in the host grain between domains I.D and I.E. Here, the linear recrystallized zones originating as kink bands developed during a late stage of the folding as

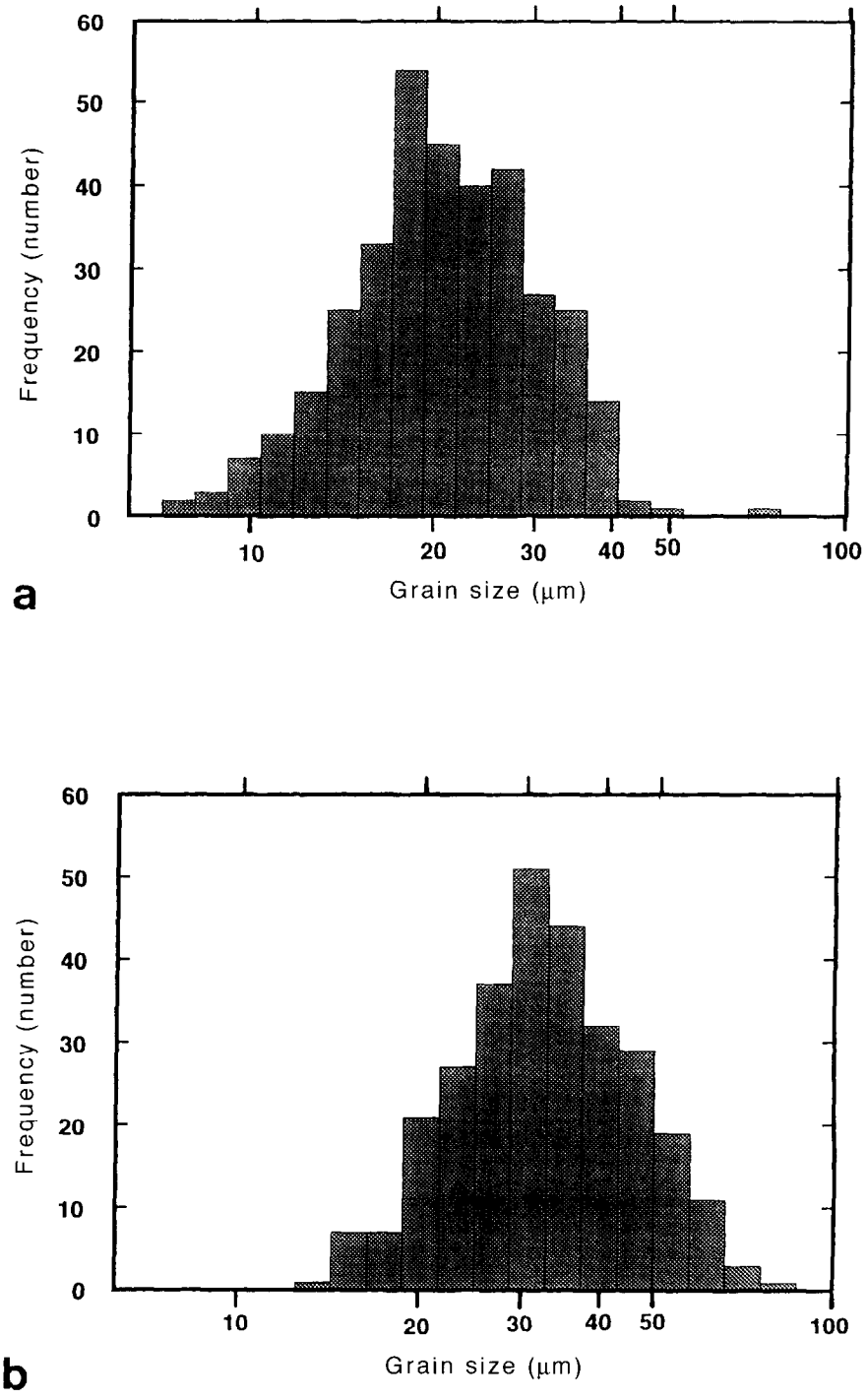

Fig. 7. Frequency distribution of recrystallized grain size in the quartz vein represented as frequency (number) vs logarithm of grain size. (a) Domains I.B and I.C (n = 348). (b) Domains II.H and II.I (n = 290).

shown by the following evidence. First, domain I.B clearly cuts the kink bands of domain I.A (Fig. 3). Second, the open microcracks were perhaps formed at a stage of decreasing temperature, and hence at a late stage of the ductile folding. Similar kink bands were reported in experimentally sheared kaolin by Margenstern and Tchalenko (1967). Accordingly, it is concluded that the linear recrystallized zones represent accommodation microstructures associated with the flexural-slip folding.

Mechanism of dynamic recrystallization inferred from the c-axis orientation distribution

In every domain from B to E in part I of the buckled quartz vein, the c-axis orientations in the

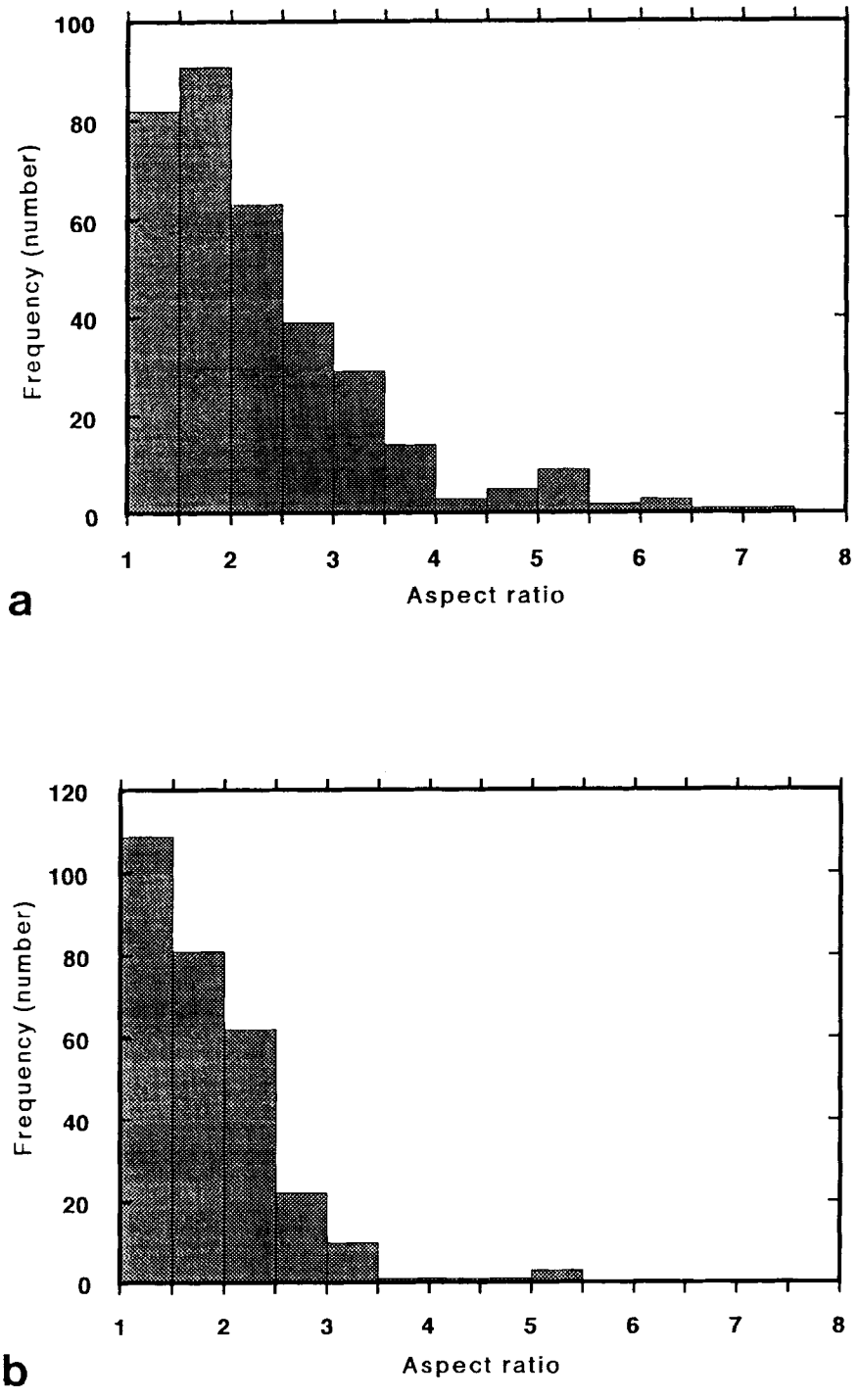

Fig. 8. Frequency distribution of aspect ratios of recrystallized grains in the quartz vein represented as frequency (number) vs aspect ratio. (a) Domains I.B and I.C (n = 348). (b) Domains II.H and II.I (n = 290).

recrystallized grains cluster around the adjacent host c-axis orientations with small misorientations mostly less than 30°, and they lie exactly on a great circle. The host-controlled c-axis orientations and trend of their variation clearly suggest that the c-axis orientations in recrystallized grains were produced by progressive subgrain rotation caused by basal (0001) slip.

There are two important features about the c-axis fabrics in part II. One is that the X-maximum c-axis fabric component was little rotated by the folding between domains II.H and II.I, while the Z-maximum c-axis fabric component was greatly rotated about the fold axis, perhaps due to the folding. The other is that the recrystallized grains exhibiting X- and Z-maximum c-axis fabric components are often adjacent to each other with large c-axis misorientations, and the former grains seem to have consumed the latter grains by grain-boundary migration (Figs 5 & 6). It can there-

Fig. 9. Grain shape fabric in a part of domain I.C of the buckled quartz vein (micrograph). Location is indicated in the inset diagram of Fig. 2. Note the shape preferred orientation of recrystallized grains, and the embayed vein–matrix interface shown by arrows and a left-over grain (L) which were presumably caused by dissolution of the quartz vein (see text). Vibration directions of crossed nicols are indicated by thick bars. Scale bar = 0.2 mm.

fore be concluded that the *X*-maximum *c*-axis fabric component was developed by grain-boundary migration (i.e. grain growth), controlled by either stress or strain field, while the *Z*-maximum *c*-axis fabric was developed by rotation recrystallization, controlled by the host *c*-axis orientation and the finite strain.

Furthermore, note that the maximum concentration of *X*-maximum *c*-axis fabric in part II, which is comparable with those reported by Hippertt (1994) and Stallard and Shelley (1995), is not very high (maximum concentration less than 5 m.u.d.), in great contrast to the strong *c*-axis fabrics (maximum concentration more than 10 m.u.d.) caused by dislocation creep in both natural quartz (e.g. Law, 1986; Pauli *et al.*, 1996) and quartz analogue material (norcamphor) (Herwegh and Handy, 1996) where dynamic recrystallization (both rotation and migration recrystallization) as well as intracrystalline slip were dominant. Therefore, the weak *X*-maximum *c*-axis fabric may be indicative of solution–precipitation (i.e. diffusion) rather than dislocation creep (also see the following discussion). In fact, the development of the *X*-maximum *c*-axis fabric is analogous to that in fibrous quartz veins formed by anisotropic grain growth from solution (e.g. Stallard and Shelley, 1995). If the migration recrystallization in the quartz was not driven by the difference in strain energy between adjacent grains, the apparent migration recrystallization is simply a solution–precipitation process.

Mechanism of dynamic recrystallization inferred from the grain microstructures

The dynamically recrystallized grain size (*ca* 32 μm) in the migration recrystallization regime (part II) is 1.5 times as large as that (*ca* 22 μm) in the rotation recrystallization regime (part I). Also, the mean aspect ratio (2.3) is higher in the rotation recrystallization regime (part I) than that (1.8) in the migration recrystallization regime (part II). These facts also indicate that the mechanism of dynamic recrystallization in the quartz can be distinguished on the basis of the recrystallized grain size and aspect ratio.

The trajectories of the longest axis of the recrystallized grains in the hinge between limbs b and c are reminiscent of those described by Hara (1971) and Hara and Paulitsch (1971) for recrystallized quartz grains in buckled quartz veins from the Sambagawa

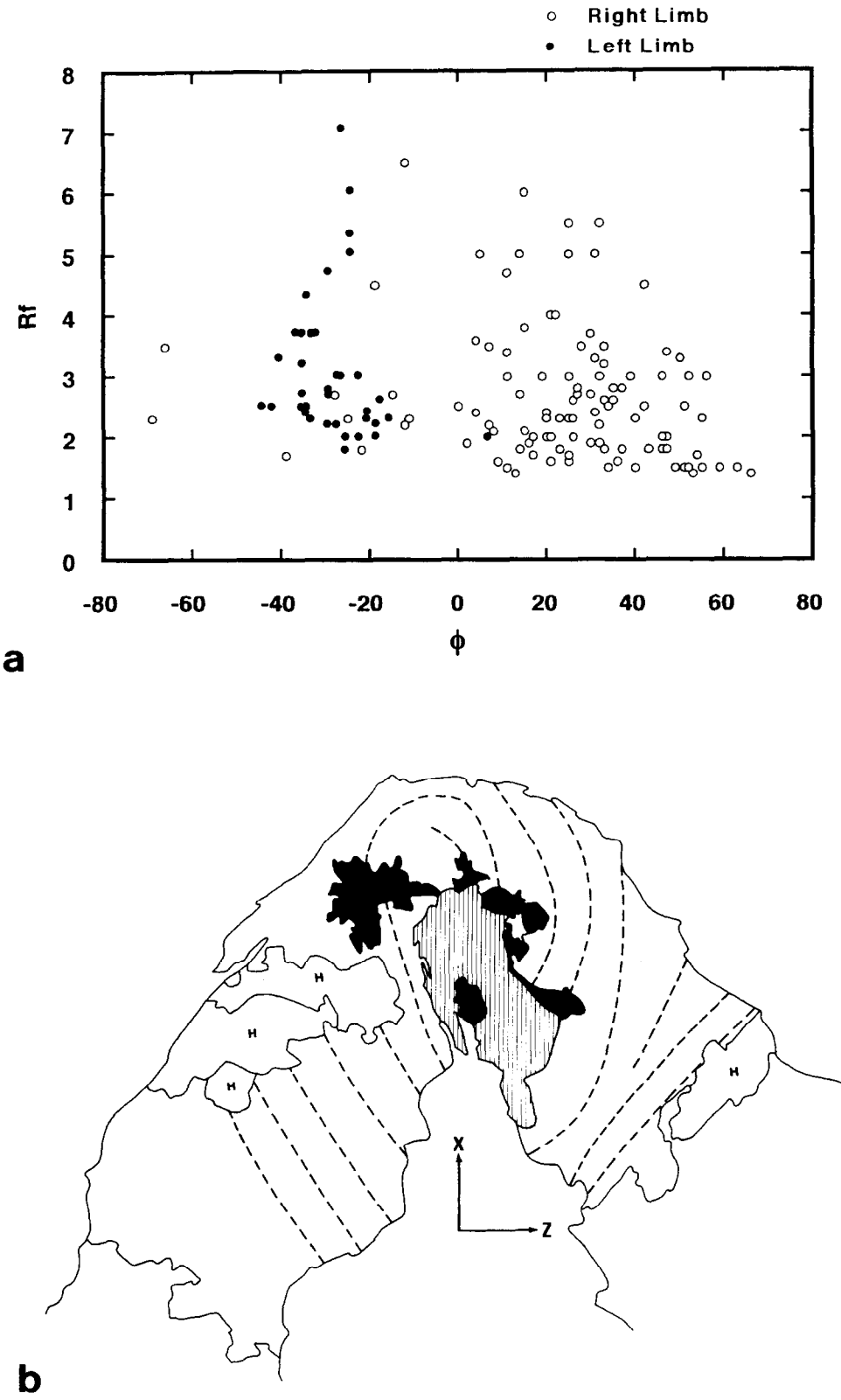

Fig. 10. (a) R_f/ϕ diagram for recrystallized grains in domains I.B and I.C (n = 149). ϕ is positive when the longest axis of recrystallized grain is rotated clockwise from the trace of the XY plane of finite strain about the fold axis. (b) Trajectories (dashed lines) of the longest axes of recrystallized grains in the same area. An area decorated by vertical thin lines denotes the discrete single crystal. H and black denote host grains and holes in the thin section, respectively. See text for further explanation.

metamorphic belt. Because those trajectories are comparable with the simulated strain pictures of Dietrich (1969) for a buckled viscous layer, they perhaps mirror the long axis of the strain ellipsoid due to the folding. Therefore, it could be concluded that in the subgrain rotation regime, the recrystallized grain shape is controlled by strain geometry.

As dissolution microstructures in the buckled quartz vein are ubiquitous, the grain-boundary migration responsible for the formation of *X*-maximum *c*-axis fabric was perhaps assisted by intergranular fluid. Boundary migration occurred by dissolution at the consumed grain boundary, diffusion of SiO_2 through the fluid and reprecipitation at the growing grain-boundary (fluid-assisted grain boundary migration, Urai *et al.*, 1986). The rate of the grain-boundary migration is considered to be limited by diffusion through the intergranular fluid film (Urai *et al.*, 1986).

The possible reason for the transition from rotation to migration recrystallization in the buckled quartz vein

The cause of the transition from rotation to migration recrystallization in the buckled quartz vein is puzzling. As discussed in the preceding sections, the weak *c*-axis fabric, lack of shape preferred orientation and ubiquitous occurrence of dissolution microstructures in recrystallized grains of part II could all indicate that solution–precipitation (i.e. diffusion) rather than dislocation creep dominated in part II. If this is true, the fluid-assisted grain-boundary migration responsible for the *X*-maximum *c*-axis fabric development could be considered as an elementary process of solution–precipitation creep. It is well known that solution–precipitation creep occurs at lower differential stresses than dislocation creep (e.g. Rutter, 1976). Therefore, it can be concluded that the magnitude of differential stress (hence strain rate) was higher in part I than in part II of the quartz vein, where dislocation creep responsible for rotation recrystallization and solution–precipitation creep responsible for migration recrystallization were dominant, respectively.

CONCLUSIONS

1. The analyzed buckled quartz vein originated as a single crystal, where the changes in host *c*-axis orientation exactly follow the bending of vein. The basal (0001) plane was nearly parallel (inclined by *ca* 10–20°) to the quartz vein surface before deformation, and the flexure (essentially kink) which produced the fold was accomplished by basal (0001) slip alone in the hinges (i.e. flexural-slip folding). Recrystallized kink bands were developed in the limbs, which are either synthetic or antithetic (conjugate) to the flexural slip. These kink bands perhaps represent accommodation microstructures associated with the flexural-slip folding.
2. Dynamic recrystallization in the quartz vein resulted from both subgrain rotation and grain-boundary migration. Rotation recrystallization associated with basal (0001) slip resulted in the host-controlled *c*-axis orientation distribution along a great circle, whereas migration recrystallization resulted in a penetrative development of a weak *X*-maximum *c*-axis fabric not rotated by the folding. The migration recrystallization is evidenced by large *c*-axis misorientations, as much as 90° across the boundaries as well as irregular grain shape. Size and aspect ratio of the recrystallized grains are larger and lower, respectively, in the migration than in rotation recrystallization regime, which also supports the operation of two different regimes of recrystallization in the quartz vein.
3. As dissolution microstructures are ubiquitous in the quartz vein, the grain-boundary migration responsible for the development of the *X*-maximum *c*-axis fabric was perhaps assisted by diffusion through intergranular fluid. The weak *c*-axis fabric development, and lack of grain shape fabric, suggests the dominance of solution–precipitation creep in the fluid-assisted grain-boundary migration regime. Hence, it is inferred that the transition from rotation to migration recrystallization regime was caused by a local decrease of differential stress in the buckled quartz vein.

Acknowledgements—We wish to thank Drs R. P. Heilbronner and M. Jessel for constructive reviews of the manuscript. We particularly thank Dr R. P. Heilbronner for suggesting to us a better way of presenting figures. We also wish to thank Professors J. Tullis and H.-R. Wenk for informal reviews of an early version of the manuscript. Dr R. J. Norris is thanked for his editorial corrections of the manuscript.

REFERENCES

Banno, S. and Sakai, C. (1989) Geology and metamorphic evolution of the Sambagawa metamorphic belt, Japan. In *Evolution of Metamorphic Belts*, eds J. S. Dely, R. A. Cliff and B. W. D. Yardley, pp. 519–532. Geological Society of London Special Publication **43**.

Blumenfeld, P., Mainprice, D. and Bouchez, J.-L. (1986) *c*-slip in quartz from subsolidus deformed granite. *Tectonophysics* **127**, 97–115.

Bouchez, J.-L. (1977) Plastic deformation of quartzites at low temperature in an area of natural strain gradient. *Tectonophysics* **39**, 25–50.

Carter, N. L. and Raleigh, C. B. (1969) Principal stress directions from plastic flow in crystals. *Bulletin of the Geological Society of America* **80**, 1231–1264.

Dieterich, J. H. (1969) Origin of cleavages in folded rocks. *American Journal of Science* **267**, 155–165.

Dunnet, D. (1969) A technique of finite-strain analysis using elliptical particles. *Tectonophysics* **7**, 117–136.

Faure, M. (1985) Microtectonic evidence for eastward ductile shear in the Jurassic orogen of SW Japan. *Journal of Structural Geology* **7**, 175–186.

Gleason, G. C., Tullis, J. and Heidelbach, F. (1993) The role of dynamic recrystallization in the development of lattice preferred orientations in experimentally deformed quartz aggregates. *Journal of Structural Geology* **15,** 1145–1168.

Guillope, M. and Poirier, J. P. (1979) Dynamic recrystallization during creep of single crystalline halite: an experimental study. *Journal of Geophysical Research* **84,** 5557–5567.

Hara, I. (1971) An ultimate steady-state pattern of *c*-axis fabric of quartz in metamorphic tectonites. *Geologische Rundschau* **60,** 1142–1173.

Hara, I., Hide, K., Takeda, K., Tsukuda, E., Tokuda, M. and Shiota, T. (1977) Tectonic movement in the Sambagawa belt. In *The Sambagawa Belt*, ed. K. Hide, pp. 309–390. Hiroshima University Press, Hiroshima, (in Japanese with English abstract).

Hara, I. and Paulitsch, P. (1971) *c*-axis fabrics of quartz in buckled quartz veins. *Neues Jahrbuch für Mineralogie Abhandlungen* **115,** 31–53.

Hara, I., Shiota, T., Hide, K., Okamoto, K., Takeda, K., Hayasaka, Y. and Sakurai, Y. (1990) Nappe structure of the Sambagawa belt. *Journal of Metamorphic Geology* **8,** 441–456.

Hara, I., Shiota, T., Hide, K., Kanai, K., Goto, M., Seki, S., Kaikiri, K., Takeda, K., Hayasaka, Y., Miyamoto, T., Sakurai, Y. and Ohtomo, Y. (1992) Tectonic evolution of the Sambagawa schist and its implications in convergent margin processes. *Journal of Science of the Hiroshima University, Series C* **9,** 495–595.

Hara, I., Uchibayashi, S., Yokota, Y., Uemura, H. and Oda, M. (1968) Geometry and internal structures of flexural folds (1), Folding of a single competent layer enclosed in thick incompetent layer. *Journal of Science of the Hiroshima University, Series C* **5,** 179–216.

Herwegh, M. and Handy, M. R. (1996) The evolution of high-temperature mylonitic microfabrics: evidence from simple shearing of a quartz analogue (norcamphor). *Journal of Structural Geology* **18,** 689–710.

Hippertt, J. F. (1994) Microstructures and *c*-axis fabrics indicative of quartz dissolution in sheared quartzites and phyllonites. *Tectonophysics* **229,** 141–163.

Hirth, G. and Tullis, J. (1992) Dislocation creep regimes in quartz aggregates. *Journal of Structural Geology* **14,** 145–159.

Hobbs, B. E. (1968) Recrystallization of single crystals of quartz. *Tectonophysics* **6,** 353–401.

Isozaki, Y. and Itaya, T. (1990) Chronology of Sambagawa metamorphism. *Journal of Metamorphic Geology* **8,** 401–411.

Kamb, W. B. (1959) Theory of preferred crystal orientation developed by crystallization under stress. *Journal of Geology* **67,** 153–170.

Kamb, W. B. (1961) The thermodynamic theory of non-hydrostatically stressed solids. *Journal of Geophysical Research* **66,** 259–271.

Karato, S.-I. (1987) Seismic anisotropy due to lattice preferred orientation of minerals: kinematic or dynamic? In: *High Pressure Research in Mineral Physics*. M. H. Manghnani and Y. Syono, eds., 455–471. American Geophysical Union, Geophysical Monograph **39**.

Law, R. D. (1986) Relationships between strain and quartz crystallographic fabrics in the Roche Maurice quartzites of Plougastel, western Brittany. *Journal of Structural Geology* **8,** 493–515.

Lister, G. S., Paterson, M. S. and Hobbs, B. E. (1978) The simulation of fabric development in plastic deformation and its application to quartzites: the model. *Tectonophysics* **45,** 107–158.

Lloyd, G. E. and Freeman, B. (1991) SEM electron channeling analysis of dynamic recrystallization in a quartz grain. *Journal of Structural Geology* **13,** 945–953.

Lloyd, G. E. and Freeman, B. (1994) Dynamic recrystallization of quartz under greenschist conditions. *Journal of Structural Geology* **16,** 867–881.

Margenstern, N. R. and Tchalenko, J. S. (1967) Microscopic structures in kaolin subjected to direct shear. *Geotechnique* **17,** 309–328.

Okudaira, T., Takeshita, T., Hara, I. and Ando, J.-I. (1995) A new estimate of the conditions for transition from basal⟨*a*⟩ to prism[*c*] slip in naturally deformed quartz. *Tectonophysics* **250,** 31–46.

Pauli, C., Schmid, S. M. and Heilbronner, R. P. (1996) Fabric domains in quartz mylonites: localized three dimensional analysis of microstructure and texture. *Journal of Structural Geology* **18,** 1183–1203.

Ramsay, J. G. (1967) *Folding and Fracturing of Rocks*. McGraw-Hill, New York, 568 pp.

Rutter, E. H. (1976) The kinetics of rock deformation by pressure solution. *Philosophical Transactions of the Royal Society of London* **A283,** 203–219.

Sander, B. (1934) Petrofabrics (Gefügekunde der Gesteine) and orogenesis. *American Journal of Science* **153,** 37–50.

Seki, S., Hara, I. and Shiota, T. (1993) Transition from flexural-flow folding to flexural-slip folding in the Sambagawa belt. *Journal of Science of the Hiroshima University, Series C* **9,** 685–696.

Stallard, A. and Shelley, D. (1995) Quartz *c*-axes parallel to stretching directions in very low-grade metamorphic rocks. *Tectonophysics* **249,** 31–40.

Takasu, A. and Dallmeyer, R. D. (1990) ^{40}Ar–^{39}Ar mineral age constraints for the tectonothermal evolution of the Sambagawa metamorphic belt, central Shikoku, Japan: a Cretaceous accretionary prism. *Tectonophysics* **185,** 111–139.

Takeshita, T. and Wenk, H.-R. (1988) Plastic anisotropy and geometrical hardening in quartzites. *Tectonophysics* **149,** 345–361.

Urai, J. L., Means, W. D. and Lister, G. S. (1986) Dynamic recrystallization of minerals. In *Mineral and Rock Deformation: Laboratory Studies*, eds B. E. Hobbs and H. C. Heard, pp. 161–199. American Geophysical Union Geophysical Monograph **36**.